

Cerebral grey matter density is associated with neuroreceptor and neurotransmitter availability: A combined PET and MRI study

Sandra Manninen^{a,*}, Tomi Karjalainen^a, Lauri J. Tuominen^{a,b}, Jarmo Hietala^c,
Valtteri Kaasinen^{d,f}, Juho Joutsa^d, Juha Rinne^a, Lauri Nummenmaa^{a,e}

^a Turku Pet Centre and Turku University Hospital, Turku, Finland

^b University of Ottawa, Institute of Mental Health Research, Ottawa, Ontario, Canada

^c Department of Psychiatry, Turku University Hospital, Turku, Finland

^d Clinical Neurosciences, University of Turku, Turku, Finland

^e Department of Psychology, University of Turku, Finland

^f Neurocenter, Turku University Hospital, Turku, Finland

ARTICLE INFO

Keywords:

MRI
Neuroreceptors
Neurotransmitters
PET
Voxel-based morphometry

ABSTRACT

Positron emission tomography (PET) can be used for *in vivo* measurement of specific neuroreceptors and transporters using radioligands, while voxel-based morphometric analysis of magnetic resonance images allows automated estimation of local grey matter densities. However, it is not known how regional neuroreceptor or transporter densities are reflected in grey matter densities. Here, we analyzed brain scans retrospectively from 328 subjects and compared grey matter density estimates with neuroreceptor and transporter availabilities. μ -opioid receptors (MORs) were measured with [¹¹C]carfentanil (162 scans), dopamine D2 receptors with [¹¹C]raclopride (92 scans) and serotonin transporters (SERT) with [¹¹C]MADAM (74 scans). The PET data were modelled with simplified reference tissue model. Voxel-wise correlations between binding potential and grey matter density images were computed. Regional binding of all the used radiotracers was associated with grey matter density in region and ligand-specific manner independently of subjects' age or sex. These data show that grey matter density and MOR and D2R neuroreceptor / SERT availability are correlated, with effect sizes (r^2) ranging from 0.04 to 0.69. This suggests that future studies comparing PET outcome measure different groups (such as patients and controls) should also analyze interactive effects of grey matter density and PET outcome measures.

1. Introduction

Neuroreceptors constitute a major class of targets for pharmacological treatments in psychiatric and neurological conditions. Positron emission tomography (PET) allows *in vivo* measurement of neuroreceptors using radioactive tracer molecules that bind to their target receptors or transporters (Heiss and Herholz, 2006). Accordingly, PET is widely used for quantifying differences in neuroreceptor availabilities across patient and control subjects to investigate pathophysiological changes in specific neurotransmitter circuits (Gryglewski et al., 2014; Volkow et al., 2009; Whone et al., 2003).

However, brain tissue composition related factors associated with radiotracer binding in humans have remained poorly understood. Mesoscopic changes in grey and white matter densities can be derived from magnetic resonance imaging using voxel-based morphometry (VBM) (Ashburner and Friston, 2000). This method is based on segmenting the T1-weighted magnetic resonance (MR) images into grey (GM) and white

matter (WM), and comparing the normalized tissue density maps across subject groups. It allows quantification of gross atrophy on the basis of the T1-weighted MR images, yet it yields molecularly unspecific results and cannot pinpoint the neuroreceptor systems involved in the tissue atrophy. The GM signal derived from structural MRI's is assumed to reflect the gross density of neurons, as a large bulk of cell bodies and neuropils (including glial cells, unmyelinated axons and dendrites) are located in grey matter (Purves, 2018). Consequently, it is possible that binding of PET receptor / transporter radioligands could be associated with the underlying mesoscopic differences in grey matter densities across subjects, as measured with VBM.

In line with this prediction, both molecular and structural neuroimaging studies have found spatially concordant alterations in the brain across multiple conditions. First, GM density declines significantly towards the old age (Resnick et al., 2003; Tang et al., 2001), and paralleling effects are also observed in opioidergic (Kantonen et al., 2020; Zubieta et al., 1999) and dopaminergic (Morgan, 1987) neurotransmitter systems, as measured with PET. Similarly, in conditions such as

* Corresponding author.

E-mail address: saalma@utu.fi (S. Manninen).

Table 1
Subject characteristics for each radioligand used in the study.

PET camera	n(males)	n(females)	Age \pm SD	Dose \pm SD	n (1.5TMRI)	N(3TMRI)
HRRT						
[¹¹ C]carfentanil	38	46	42 \pm 9	468 \pm 59	45	39
[¹¹ C]MADAM	33	41	43 \pm 12	490 \pm 30	37	37
[¹¹ C]raclopride	35	0	24 \pm 2	299 \pm 62	7	28
PET-CT						
[¹¹ C]carfentanil	10	14	36 \pm 14	252 \pm 10	14	10
[¹¹ C]raclopride	0	20	43 \pm 15	253 \pm 17	20	0
PET-MRI						
[¹¹ C]carfentanil	54	0	25 \pm 5	251 \pm 14	0	54
ECAT						
[¹¹ C]raclopride	4	11	62 \pm 10	198 \pm 15	15	0
HR+						
[¹¹ C]raclopride	0	19	23 \pm 4	309 \pm 112	19	0
GE-advance						
[¹¹ C]raclopride	0	3	54 \pm 8	182 \pm 4	3	0

morbid obesity where significant cerebral atrophy is found using VBM (Karlsson et al., 2013; Tuulari et al., 2016), PET studies show down-regulation of opioid (Karlsson et al., 2016; Karlsson et al., 2015) and possibly also D2-like dopamine receptors (Wang et al., 2001). Numerous psychiatric conditions including major depression are also associated with significant cerebral atrophy (Goodkind et al., 2015) and also regional downregulation of specific neurotransmitters, such as the serotonergic (Gryglewski et al., 2014; Spies et al., 2015) and opioidergic (Kennedy et al., 2006; Nummenmaa et al., 2020) systems. Finally, correlational studies linking brain scans with behavior also suggest linkage between grey matter densities and radioligand binding. For example, personality traits associated with prosociality are positively associated with both increased frontal cortical volumes (Lewis et al., 2011; Manninen et al., 2017) and μ -opioid receptor (MOR) availability corresponding regions, as measured with PET (Nummenmaa et al., 2015; Nummenmaa et al., 2016). Few previous studies have already proved a positive correlation with grey matter density and receptor availability with certain (dopamine- and serotonin) receptors (Kraus et al., 2012; Woodward et al., 2009). These studies however investigated single tracers with small sample sizes. Here, the focus is to reveal a possible link between grey matter density and receptor availability in whole brain area with 3 different tracers to reveal whether tracer uptake and brain density are associated in receptor and transporter specific fashion.

1.1. The current study

The objective of the current study was to investigate the potential links between availability of specific neuroreceptors and transporters measured with PET and grey matter density measured with VBM and MRI. We focused specifically on μ -opioid and dopamine D2-like receptors and serotonin transporters, as these systems have different and yet partially overlapping distributions in the brain (Chalon et al., 2003; Egerton et al., 2009; Frost et al., 1985). We pooled together data from altogether 328 adults who had undergone a PET study with one radioligand each, as well as structural MR imaging with a T1-weighted sequence. We computed voxel-wise as well as region-of-interest based association between GM density and ligand-wise outcome measures. We found that receptor and transporter availabilities were positively associated with GM density in regionally specific fashion for each ligand, and these effects were also independent of age and sex related changes.

2. Materials and methods

2.1. Subjects

The data (see Table 1) were historical subjects studied at Turku PET Centre between 1998 and 2016. Altogether 328 subjects' (154 females, age range 18–74 years, $M_{age} = 35.8$ years, $SD_{age} = 13.9$ years) scans

were included in the study, with a total of 162 [¹¹C]carfentanil, 74 [¹¹C]MADAM, and 92 [¹¹C]raclopride scans (Table 1). The study was conducted in accordance with the Helsinki Declaration. Because the study was a retrospective, register based investigation of historical data, informed consent was waived. The study protocol was reviewed by the institutional review board of the Hospital District of South-Western Finland. The subject-pool consisted primarily (82 %) of healthy controls but included also patients, and this distribution varied slightly across the three ligands. There proportion of controls from the total sample was 139 / 162 subjects for carfentanil (23 morbidly obese subjects), 48 / 74 subjects for MADAM (24 pathological gamblers and patients with gambling addiction) and 80 / 92 subjects for raclopride (12 patients with Parkinson's disease or Alzheimer's disease). For the sake of brevity, we included all eligible scans (controls and patients) in the dataset. To rule out potential disease-related confounds in the results, patient versus control status was controlled for in the analyses.

2.2. MRI and PET data acquisition

Anatomical MR images (voxel size 1 mm³) were acquired with Philips Gyroscan Intera 1.5T scanner or Philips Ingenuity 3T PET/MR scanner using T1-weighted sequences. PET data were acquired with the Philips Ingenuity PET/MR scanner, GE Healthcare Discovery 690 PET/CT scanner (General Electric Medical Systems, Milwaukee, WI, USA), GE Advance, CTI-Siemens ECAT EXACT HR+ , Siemens HR+ and brain-dedicated high-resolution PET scanner (ECAT HRRT, Siemens Medical Solutions in Turku PET Centre). MOR availability was measured with [¹¹C]carfentanil, D2R availability with [¹¹C]raclopride and SERT availability with [¹¹C]MADAM.

2.3. MRI data preprocessing for voxel-based morphometry

Prior to analysis, the image quality was checked visually and the origo of each T1-weighted image was set to anterior commissure. Structural images were analyzed with SPM12 (www.fil.ion.ucl.ac.uk/spm/) software and its DARTEL pipeline that first creates a study-specific template and for grey and white matter based on the normalized subject-wise input data, and normalizes the subject-wise images using these templates. Default parameter values were used in the DARTEL analysis while preserving concentration. The DARTEL-normalized GM images were resampled into 2 mm isotropic voxel size and smoothed using a Gaussian kernel of 6 mm full width at half maximum (FWHM).

2.4. PET data preprocessing

To correct for head motion, PET images were first realigned frame-to-frame. Next, they were co-registered with the anatomical MR images. Tracer-wise reference regions (medial occipital cortex for

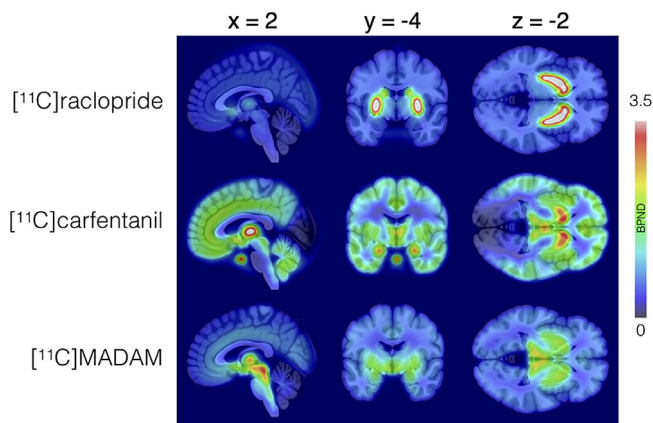


Fig. 1. Mean BP_{ND} -map for each tracer shown over T1-weighted structural MR template image.

$[^{11}C]$ carfentanil and cerebellum for $[^{11}C]$ MADAM and $[^{11}C]$ raclopride) were automatically defined using FreeSurfer parcellations from the anatomical MR images. The resulting parcellations for occipital and cerebellar grey matter were slightly compressed to avoid spillover from adjacent white matter and grey matter regions with specific binding (Karjalainen et al., 2020). Neuroreceptor/-transporter availability was expressed in terms of BP_{ND} , which is the ratio of specific to non-displaceable binding in brain. BP_{ND} was calculated applying a basis function method for each voxel using the simplified reference tissue model (Gunn et al., 1997). BP_{ND} is not confounded by differences in peripheral distribution or radiotracer metabolism. For the employed radiotracers, the BP_{ND} is traditionally interpreted by target molecule density (B_{max}), even though $[^{11}C]$ carfentanil and $[^{11}C]$ raclopride are also sensitive to endogenous neurotransmitter activation. Accordingly, the BP_{ND} for these radiotracers should be interpreted as availability of receptors, which in turn is an indirect index of density of available receptors (B_{avail}). Resulting subject-wise parametric BP_{ND} images were then spatially normalized using the individual flow fields derived from the DARTEL analysis, resampled into 2mm isotropic voxel size to match with the GM segments, and finally smoothed with a Gaussian kernel of 6 mm FWHM. Fig. 1 shows the mean BP_{ND} distribution for each radioligand.

2.5. Data analysis

We computed the associations between mean GM density and BP_{ND} 's in selected a priori regions of interest (ROIs) including amygdala, caudate, orbitofrontal cortex (OFC), putamen, thalamus and ventral striatum (VS); see SI for complementary full-volume analysis. The ROIs were delineated manually on the mean tracer-specific grey matter DARTEL templates. To control for the effect of potential confounders for the association between BP_{ND} and GMD (age, MRI scanner and PET cameras and their interactions) the ROI analyses were performed using linear mixed models (LMMs) with R statistical software (<https://cran.r-project.org>) and *lme4* package. The model ($BP_{ND} \sim (1 | \text{PET scanner}) + (1 | \text{Patient/Control group}) + 1 + \text{Age} * \text{GMD} + \text{GMD} * \text{MRI scanner}$) included scanners and patient / control groups as random effect. Because all MADAM data came from a single PET scanner, this term was dropped from the corresponding analyses. Complementary full-volume analyses are described in the SI file.

3. Results

Radioligand-specific regional BP_{ND} and corresponding regional grey matter densities are shown in Fig. 2. All $[^{11}C]$ MADAM data came from

a single PET camera, and BP_{ND} estimates for $[^{11}C]$ carfentanil were consistent across cameras, with largest variability in the amygdala. Camera-wise estimates were also comparable for $[^{11}C]$ raclopride, with the main exception being lower binding potentials in images scanned with the ECAT camera.

The overall pattern of association between BP_{ND} and GMD are shown in Fig. 3 (see Figure S-3 for data factored by PET camera). As different scanners yielded slightly different binding estimates (despite using BP_{ND} as the outcome measure), we used linear mixed model (LMM) to predict regional BP_{ND} with GMD while accounting for age, MRI scanner, PET camera and their interactions. This revealed that although there were scanner disparities and age dependent effects on BP_{ND} , these did not account for the association between regional BP_{ND} and GMD (Table 2): For $[^{11}C]$ carfentanil, significant positive associations were found in amygdala, caudate, thalamus and ventral striatum. Negative association was found in the OFC. For $[^{11}C]$ raclopride, positive association was found in all tested regions (caudate, putamen, thalamus and ventral striatum). For $[^{11}C]$ raclopride, positive association were found in amygdala, caudate, thalamus and ventral striatum, while the association was negative in putamen. Restricting the sample to include only the controls yielded comparable results (Table S-2).

Although the reference tissue model theoretically controls for differences across PET cameras, it has been established that comparable PET scanning protocols yield different BP_{ND} estimates across scanners, particularly for the HRRT camera used in our sample (van Velden et al., 2015). In addition to modelling the effect of PET camera in the LMM analyses, we thus conducted a separate analysis using a single-camera dataset; HRRT was chosen for this purpose as it was used with all the radioligands (and it was the only camera yielding $[^{11}C]$ MADAM data). This analysis (Table S-3) yielded estimates highly similar to those obtained using the whole sample, suggesting that variability across scanners does not explain the association between grey matter density and binding potential. Due to volumetric differences the ROIs also vary in signal-to-noise ratio as well as in how they suffer from partial volume effect. Thus, we also computed correlations between the ROI size (in voxels) and mean regional i) GM density, ii) BP_{ND} and iii) the GM density \times BP_{ND} association. The effects were in general negative (Table S-4), suggesting that both BP_{ND} and GMD estimates were highest in smallest ROIs, and that the association between BP_{ND} and GMD was also largest in the smallest region with highest signal.

4. Discussion

Our main finding was that there is a significant positive association between GM density and BP_{ND} with all tested radiotracers. With $[^{11}C]$ raclopride the association was strongest in the striatum, and with $[^{11}C]$ carfentanil and $[^{11}C]$ MADAM in the striatum, thalamus and amygdala. The effects remained essentially unchanged even when controlling for age and sex, which are known to influence both GM and the neuroreceptor systems (Kantonen et al., 2020; Resnick et al., 2003). In comparison with previous investigations on GM density and radiotracer uptake, we also observed effects with significantly larger number of regions likely due to improved statistical power (Kraus et al., 2012; Woodward et al., 2009). In general, the association between GMD and BP_{ND} were of moderate magnitude. Effect sizes (r^2) of grey matter density on BP_{ND} were in the rank of 0.1 for $[^{11}C]$ carfentanil, 0.2 for $[^{11}C]$ raclopride and 0.15 for $[^{11}C]$ MADAM when the raw BP_{ND} and GMD were considered; the LMM yielded T-scores ranging from 1.88 to 4.43. Although these effects were smaller when controlling for other confounds, they are still considerable given that e.g. 10 % between-groups difference in neuroreceptor availability is already substantially large. Altogether these results suggest that availability of these neuroreceptors and transporters, as measured with PET, is reflected in the density of the cerebral tissue as measured with MRI.

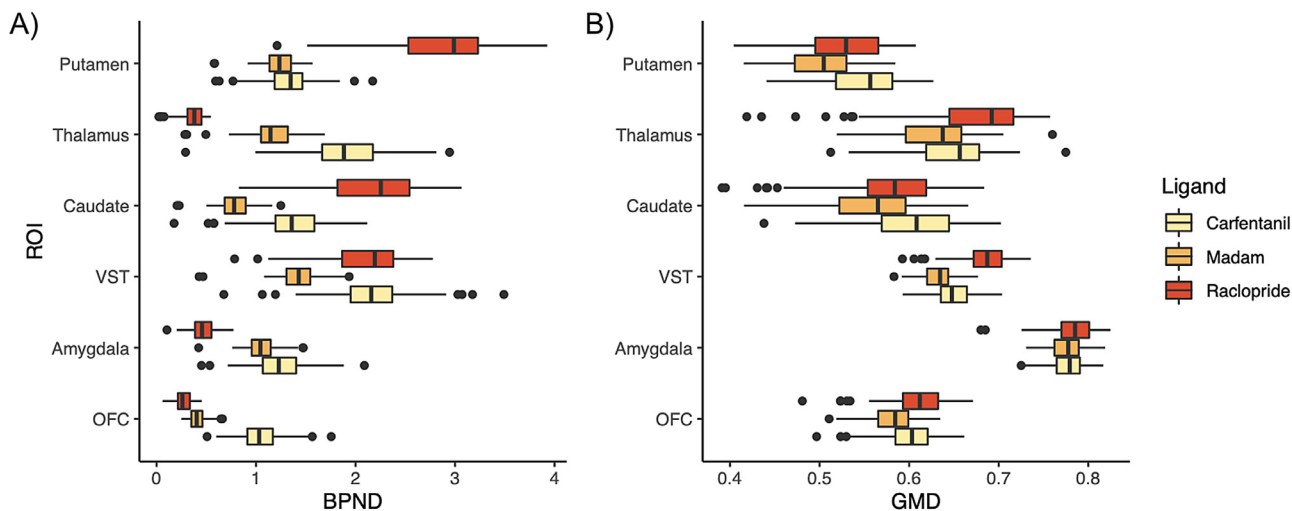


Fig. 2. ROI-wise distributions of BP_{ND} 's (A) and mean grey matter densities (GMD) for subjects scanned with each tracer. [^{11}C]raclopride does not have specific binding outside the striatum, but the mean values are shown for the sake of comparison. Note: these values are raw BP_{ND} thus potential variation related to confounders has not been partialled out.

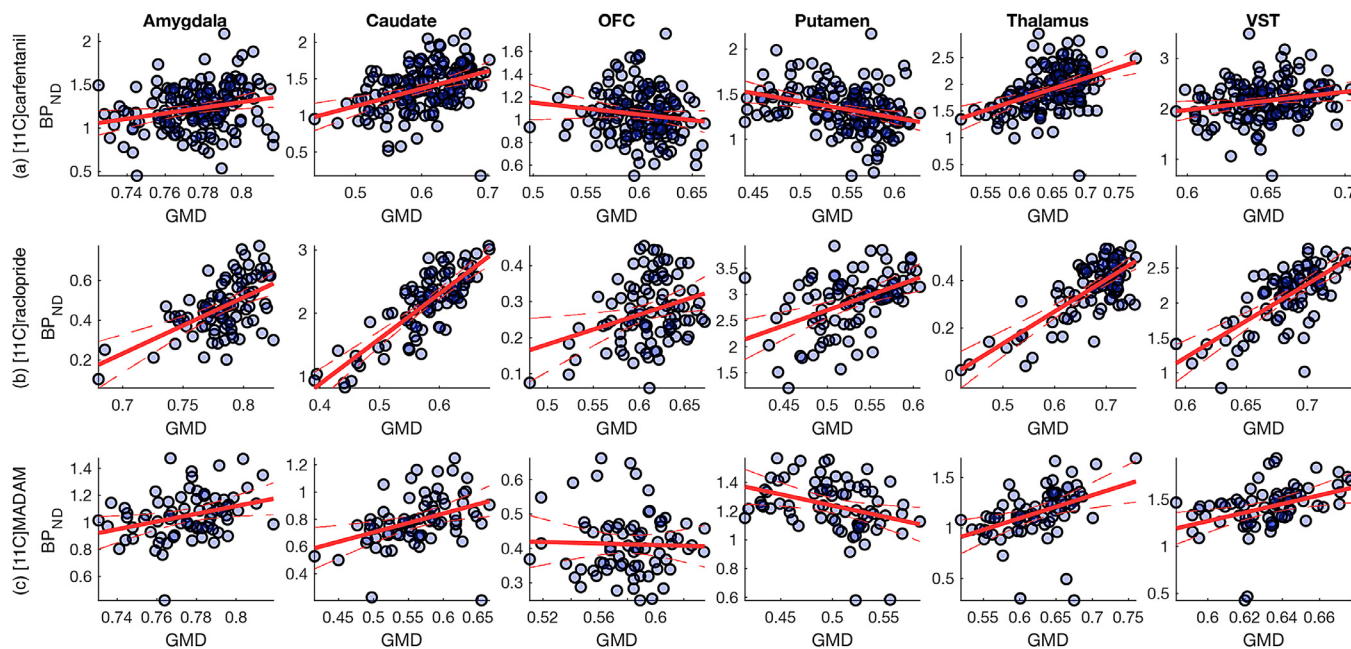


Fig. 3. Regional associations and least-squares regression lines between GM density and BP_{ND} for all tracers. Note: plots visualize association between raw BP_{ND} / GMD, thus variation related to confounders has not been regressed out from the values.

4.1. Effects of grey matter density on receptor availability

Because MRI-based GM estimate is unspecific with respect to the neuroreceptor and transporter expressions in the neurons in the tissue, we expected to see unique spatial distribution of the GM density and BP_{ND} associations for each radiotracer, and not simply significant coupling for all radiotracers in regions with VBM tissue densities. This assumption was confirmed by our data. We observed positive correlations with BP_{ND} and GM density with all tracers even though the spatial distribution of these effects varied from tracer to tracer. In line with our predictions, mesoscopic variation in grey matter density was positively associated with radioligand-specific BP_{ND} (that can be presumed to reflect the amount of available receptors in the target tissue). The consistency of these effects was validated in multiple ways, as they were replicate i) when partial volume effects were controlled for (see SI file),

ii) in a sample consisting only of healthy controls and iii) in a sample scanned with a single (HRRT) PET camera.

The most straightforward explanation for the effects is that GM density correlated with receptor / tracer density, because higher grey matter density has larger capacity for receptor / transporter expression. However, one post mortem study found that striatal dopamine transporter availability was not associated with the density of nigral neuron, which project to the striatum (Saari et al., 2017). Neurotransmission system alterations are typically related to common degenerative brain diseases: dopamine dysfunctions in nigral area and changes in opioid receptor availability are involved in Parkinson's disease (Heiss and Hilker, 2004; Piccini et al., 1997) and on the other hand, synaptic loss and serotonergic dysfunction correlates with severity of the symptoms in Alzheimer's disease (Heiss and Herholz, 2006; Terry, 2000). Accordingly, it is possible that a functional neurotransmission is dependent on available and

Table 2

Results of linear mixed models where regional ligand-specific BP_{ND} were predicted with age, GMD, MRI and PET scanners and their interactions when applicable. Effects whose SE:s do not overlap zero are shown in boldface. Note: Amygdala and orbitofrontal cortex are not analyzed for [^{11}C]raclopride due to lack of specific binding in these regions.

		$[^{11}C]$ carfentanil			$[^{11}C]$ raclopride			$[^{11}C]$ MADAM		
		Estimate	SE	T	Estimate	SE	T	Estimate	SE	T
Amygdala	Age	-0.09	0.02	-4.32				-0.01	0.02	-0.60
	GMD	0.04	0.02	2.02				0.05	0.02	2.47
	MRI scanner 1	0.19	0.04	5.10						
	MRI scanner 2									
	Age X GMD	0.00	0.01	0.27				-0.01	0.02	-0.39
	GMD X MRI scanner 1	0.00	0.03	0.03						
	GMD X MRI scanner 2									
Caudate	Age	0.07	0.03	2.69	-0.09	0.03	-3.30	0.00	0.03	-0.04
	GMD	0.12	0.03	4.35	0.18	0.03	5.92	0.09	0.03	2.78
	MRI scanner 1	0.22	0.05	4.07	0.16	0.05	3.47			
	MRI scanner 2				0.07	0.13	0.51			
	Age X GMD	-0.02	0.02	-0.73	-0.02	0.02	-1.27	0.02	0.03	0.48
	GMD X MRI scanner 1	0.04	0.04	0.81	-0.10	0.04	-2.47			
	GMD X MRI scanner 2				-0.02	0.05	-0.30			
OFC	Age	0.06	0.02	2.39				0.02	0.03	0.55
	GMD	-0.04	0.02	-1.70				0.00	0.03	-0.04
	MRI scanner 1	0.16	0.04	4.42						
	MRI scanner 2									
	Age X GMD	0.03	0.01	2.04				-0.03	0.02	-1.12
	GMD X MRI scanner 1	0.03	0.03	0.90						
	GMD X MRI scanner 2									
Putamen	Age	0.04	0.02	2.03	-0.08	0.03	-2.52	0.00	0.02	0.06
	GMD	0.02	0.04	0.45	0.09	0.04	2.26	0.05	0.02	-1.98
	MRI scanner 1	0.22	0.05	4.43	0.08	0.06	1.43			
	MRI scanner 2				-0.11	0.13	-0.87			
	Age X GMD	0.02	0.02	0.76	0.02	0.03	0.89	0.01	0.03	-0.21
	GMD X MRI scanner 1	0.00	0.05	0.08	-0.04	0.04	-0.93			
	GMD X MRI scanner 2	-	-	-	-0.13	0.08	-1.66			
Thalamus	Age	-0.05	0.02	-2.16	-0.09	0.06	-1.55	0.00	0.04	-0.10
	GMD	0.04	0.02	1.82	0.29	0.07	4.40	0.08	0.03	2.24
	MRI scanner 1	0.11	0.04	2.56	0.12	0.09	1.38			
	MRI scanner 2				-0.15	0.21	-0.74			
	Age X GMD	0.00	0.02	0.24	0.06	0.04	1.78	-0.03	0.04	-0.74
	GMD X MRI scanner 1	0.05	0.03	1.36	-0.17	0.08	-2.05			
	GMD X MRI scanner 2				-0.32	0.09	-3.57			
VS	Age	-0.03	0.02	-1.66	-0.05	0.03	-1.37	0.01	0.03	0.36
	GMD	0.04	0.02	2.23	0.10	0.03	3.16	0.08	0.03	2.99
	MRI scanner 1	0.19	0.04	4.93	0.02	0.05	0.48			
	MRI scanner 2				-0.31	0.14	-2.20			
	Age X GMD	0.00	0.02	-0.12	0.01	0.02	0.42	0.02	0.02	-0.80
	GMD X MRI scanner 1	0.01	0.03	0.20	-0.04	0.04	-0.84			
	GMD X MRI scanner 2				-0.18	0.06	-2.95			

functioning receptors on the neuron cell surface and not solely the exact amount of the neurons. Furthermore, all neurons don't necessarily express the same amount of different transmitters' receptors in central nervous system. Future studies resolving this discrepancy would be important. If higher grey matter density simply reflects larger capacity for receptor and transporter expression, PET findings in longitudinal studies where grey matter loss is pronounced would be deemed unspecific, as they might only reflect trivial changes in grey matter atrophy. However, if receptor activity would actually modulate brain morphology, the PET data would have high specificity and would thus provide complementary information to the grey matter densities.

We also unexpectedly observed negative associations between radioligand binding and GM density in the putamen for [^{11}C]MADAM and OFC for [^{11}C]carfentanil. We have no clear explanation for this effect, but it has been previously speculated that such effects may reflect regional differences in the regional neurotransporter / receptor availabilities, or the consistency of the segmentation of the T1-weighted images (Kraus et al., 2012; Woodward et al., 2009). Or, when the regional GM density grows, there might be relatively more such neurons, that don't express those neurotransmitter's receptors in question.

Finally, in some regions (such as caudate) we observed a positive association with GM density and all BP_{ND} of all the radiotracers. This

is not unexpected, as VBM-based grey matter density indices the gross number of cell bodies and neuropil (Purves, 2018), and single GM voxel may contain tens of thousands of glial cells and neurons with different receptor expression profiles. It is well known that the VBM-based density metrics are difficult to interpret on their own (Zatorre et al., 2012) and the present data shows that intersubject variability in neuroreceptor and transporter availability may influence these MR-driven metrics. In any case, from methodological perspective these finding suggest that mere (unspecific) grey matter differences might confound concomitant neuro-receptor-level changes between, for example, patient and control groups. Hence, it would be advisable to statistically test the unique effects of group membership and underlying grey matter atrophy in neuroreceptor PET studies. Altogether these results thus suggest that BP_{ND} and GM densities are coupled: If someone has high grey matter tissue density, he/she also likely has high tracer binding potentials (expect for in putamen for raclopride and MADAM). However, this association can be manifested in both regions having high and low BP_{ND} or GM density, thus it not simply driven by high-binding areas in PET or high-density areas in in MR. We also stress that this coupling is far from complete, as the correlations between BP_{ND} and GM densities vary from 0.22 to 0.83. The proportion of GMD not accounted a radiotracer's BP_{ND} likely reflects both error variance and presence of neurons operating with other

neurotransmitters within each GMD voxel, yet these effects cannot be partialled out in the current design where each subject was scanned with a single radioligand.

4.2. Effects of age on brain morphology and neuroreceptor level changes

Atrophy and synaptic loss are consistently observed in healthy aging brain (Gunning-Dixon et al., 2009; Peelle et al., 2012; Resnick et al., 2003), but also contributing to degenerative late age pathologies such as Alzheimer's and Parkinson's diseases (Alves et al., 2013; Bellucci et al., 2016; Benson et al., 1988; Terry, 2000). Similarly, specific neurotransmitter systems show age-dependent alterations. While dopamine D2 (Antonini et al., 1993; Rinne et al., 1993) and serotonin transporter (van Dyck et al., 2000) densities decrease during aging, an opposite pattern is observed for μ -opioid receptors (Kantonen et al., 2020). Analysis of the associations between ligand-specific BP_{ND} and GM density revealed strong regional association that were, to some extent, modulated by age and sex. However, the overall pattern of results (i.e. association between BP_{ND} 's and GM densities) remained essentially unchanged even when controlling for age and sex, thus the association cannot be explained by age-dependent atrophy that would lower radiotracer binding in general. Our subjects' were primarily young and middle-aged adults (mean age 35.8 years), and effects of age-dependent atrophy on radiotracer uptake might be observed only in significantly older subjects. Nevertheless the fusion analysis suggests that joint analysis of cerebral atrophy (VBM) and receptor/transporter systems could be useful in tracking the development of neurological and psychiatric conditions: Regional volumetric brain changes are associated with specific neuropsychological symptoms, and also to specific neurotransmitter system alterations. The presently observed linkage between transporter and receptor densities highlights that it is imperative to investigate how the linkage is manifested across neurological and psychiatric pathologies.

4.3. Limitations

We combined retrospective data from several different studies performed with different scanners, and the dataset was also heterogeneous with respect to subject age, sex and radiotracer dosage. However, calibrated PET scanners yield consistent data (Johansson et al., 2013) and the employed outcome measure (BP_{ND}) should theoretically control for minor differences in scanner signal-to-noise ratios (Gunn et al., 1997). In line with this, the effects were significant even though we controlled for scanner type. However there was still evidence for differential effects depending on the scanner. Despite this, even BP_{ND} estimates are known to vary between-scanner differences may be amplified depending on implemented PVEc (Schain et al., 2012). Thus, caution should be warranted when combining data across PET cameras, and the dependencies between camera types and independent variables (such as age, sex, and patient status) should be taken into account and optimally controlled for when building up the pooled sample. The scans for different radioligands came from different subjects, so individual differences in the tracer-specific samples might also confound the results. The dataset also included patients, and proportion of patients varied across ligands (12% for raclopride, 15% for carfentanil, 33% for MADAM). Although this might introduce confounds, we validated that results using a controls-only sample yielded consistent results. The direct causal linkage between the neuroreceptor and transporter availability and GM density cannot be established using the current cross-sectional data, thus we do not know if increase in the number of density of specific neuroreceptors or transporters would yield increase in the GM signal in MR. Future translational and animal imaging studies are needed for elucidating this aspect. Finally, future studies could address the relationship between receptor and transporter density and other MRI-derived metrics, such as grey matter density estimated with surface analyses.

5. Conclusions

We conclude that regional binding of [11 C]carfentanil, [11 C]raclopride and [11 C]MADAM is associated with grey matter density at the binding site. Grey matter density and tracer BP_{ND} are associated in region and ligand-specific manner for [11 C]carfentanil, [11 C]raclopride and [11 C]MADAM. These data thus suggest that VBM signal partially reflects neuroreceptor and transporter levels, and also suggests that when comparing any PET outcome measure across two groups, it is advisable to consider GM density differences between the group as well.

Data availability

Per current Finnish legislation and research permission the dataset cannot be publicly shared.

Pre-processing of the PET data as well as its kinetic modelling were done using Magia toolbox, for which the code is available in <https://github.com/tkjarjal/magia>. Volumetric results files are available in Neurovault at <https://neurovault.org/collections/JOGHJBVA/>. According to Finnish privacy protection legislation, individual participant-level study data cannot be made openly available for the scientific community, even after pseudonymization. Specific consent from the study subjects for any "further use" would be required. If needed, coded participant-level data from our study can be made available to the Journal and its reviewers, but this must be based on a confidentiality agreement.

Author contributions

Designed the study: TK, LT, JR, LN.
Acquired data: SM, LT, JH, VK, JJ, JR.
Analyzed the data: SM, TK.
Wrote the manuscript: SM, TK, LJT, JH, VK, JJ, JR, LN.

Declaration of Competing Interest

The authors declare no conflict of interest.

Acknowledgments

This work was supported by the Academy of Finland (grants #304385, #294897, and #332225) and Sigrid Juselius Foundation grants to LN, and the Alfred Kordelin Foundation grant to SM, and Päivikki and Sakari Sohlberg Foundation and Finnish Cultural Foundation Varsinais-Suomi Regional Fund to TK. We thank Tuulia Malen, Jouni Tuisku, and Severi Santavirta for their help with the data analysis.

Supplementary materials

Supplementary material associated with this article can be found, in the online version, at doi:10.1016/j.neuroimage.2020.117520.

References

- Alves, J., et al., 2013. Posterior cortical atrophy and alzheimer's disease: a meta-analytic review of neuropsychological and brain morphometry studies. *Brain Imaging Behav.* 7, 353–361.
- Antonini, A., et al., 1993. Effect of age on D(2)-dopamine receptors in normal human brain measured by positron emission tomography and C-11 raclopride. *Arch. Neurol.* 50, 474–480.
- Ashburner, J., et al., 2000. Voxel-based morphometry - the methods. *Neuroimage* 11, 805–821.
- Bellucci, A., et al., 2016. Review: Parkinson's disease: from synaptic loss to connectome dysfunction. *Neuropathol. Appl. Neurobiol.* 42, 77–94.
- Benson, D.F., et al., 1988. Posterior cortical atrophy. *Arch. Neurol.* 45, 789–793.
- Chalon, S., et al., 2003. Pharmacological Characterization of N,N-dimethyl-2-(2-amino-4-methylphenyl thio)benzylamine as a ligand of the serotonin transporter with high affinity and selectivity. *J. Pharmacol. Exp. Ther.* 304, 81–87.

- Egerton, A., et al., 2009. The dopaminergic basis of human behaviors: a review of molecular imaging studies. *Neurosci. Biobehav. Rev.* 33, 1109–1132.
- Frost, J.J., et al., 1985. Imaging opiate receptors in the human brain by positron tomography. *J. Comput. Assist. Tomogr.* 9, 231–236.
- Goodkind, M., et al., 2015. Identification of a common neurobiological substrate for mental illness. *JAMA Psychiatry* 72, 305–315.
- Gryglewski, G., et al., 2014. Meta-analysis of molecular imaging of serotonin transporters in major depression. *J. Cereb. Blood Flow Metab.* 34, 1096–1103.
- Gunn, R.N., et al., 1997. Parametric imaging of ligand-receptor binding in pet using a simplified reference region model. *Neuroimage* 6, 279–287.
- Gunning-Dixon, F.M., et al., 2009. Aging of cerebral white matter: a review of MRI findings. *Int. J. Geriatr. Psychiatry* 24, 109–117.
- Heiss, W.D., et al., 2006. Brain receptor imaging. *J. Nucl. Med.: Off. Publ., Soc. Nucl. Med.* 47, 302–312.
- Heiss, W.D., et al., 2004. The sensitivity of 18-fluorodopa positron emission tomography and magnetic resonance imaging in Parkinson's disease. *Eur. J. Neurol.* 11, 5–12.
- Johansson, J., et al., 2013. Image quantification in high-resolution pet assessed with a new anthropomorphic brain phantom. 2013 IEEE Nuclear Science Symposium and Medical Imaging Conference. Ieee, New York.
- Kantonen, T., et al., 2020. Interindividual variability and lateralization of M-opioid receptors in the human brain. *Neuroimage*.
- Karjalainen, T., et al., 2020. Magia: robust automated modeling and image processing toolbox for pet neuroinformatics. *Front. Neuroinform.*, 604835.
- Karlsson, H.K., et al., 2016. Weight loss after bariatric surgery normalizes brain opioid receptors in morbid obesity. *Mol. Psychiatry* 21, 1057–1062.
- Karlsson, H.K., et al., 2015. Obesity is associated with decreased Mu-opioid but unaltered dopamine D-2 receptor availability in the brain. *J. Neurosci.* 35, 3959–3965.
- Karlsson, H.K., et al., 2013. Obesity is associated with white matter atrophy: a combined diffusion tensor imaging and voxel-based morphometric study. *Obesity* 21, 2530–2537.
- Kennedy, S.E., et al., 2006. Dysregulation of endogenous opioid emotion regulation circuitry in major depression in women. *Arch. Gen. Psychiatry* 63, 1199–1208.
- Kraus, C., et al., 2012. Serotonin-1a receptor binding is positively associated with gray matter volume - a multimodal neuroimaging study combining pet and structural Mri. *Neuroimage* 63, 1091–1098.
- Lewis, P.A., et al., 2011. Ventromedial prefrontal volume predicts understanding of others and social network size. *Neuroimage* 57, 1624–1629.
- Manninen, S., et al., 2017. Social laughter triggers endogenous opioid release in humans. *J. Neurosci.* 37, 6125–6131.
- Morgan, D.G., 1987. The dopamine and serotonin systems during aging in human and rodent brain - a brief review. *Progr. Neuro-Psychopharmacol. Biol. Psychiatry* 11, 153–157.
- Nummenmaa, L., et al., 2020. Lowered endogenous Mu-opioid receptor availability in subclinical depression and anxiety. *Neuropsychopharmacol.: Off. Publ. Am. Coll. Neuropsychopharmacol.*
- Nummenmaa, L., et al., 2015. Adult attachment style is associated with cerebral M-opioid receptor availability in humans. *Hum. Brain Mapp.* 36, 3621–3628.
- Nummenmaa, L., et al., 2016. Social touch modulates endogenous M-opioid system activity in humans. *Neuroimage* 138, 242–247.
- Peelle, J.E., et al., 2012. Adjusting for global effects in voxel-based morphometry: gray matter decline in normal aging. *Neuroimage* 60, 1503–1516.
- Piccini, P., et al., 1997. Alterations in opioid receptor binding in Parkinson's disease patients with levodopa-induced dyskinesias. *Ann. Neurol.* 42, 720–726.
- Purves, D., 2018. *Neuroscience*. Oxford University Press, Oxford.
- Resnick, S.M., et al., 2003. Longitudinal magnetic resonance imaging studies of older adults: a shrinking brain. *J. Neurosci.* 23, 3295–3301.
- Rinne, J.O., et al., 1993. Decrease in human striatal dopamine-D2 receptor density with age - a pet study with C-11 raclopride. *J. Cereb. Blood Flow Metab.* 13, 310–314.
- Saari, L., et al., 2017. Dopamine transporter imaging does not predict the number of nigral neurons in Parkinson disease. *Neurology* 88, 1461–1467.
- Schain, M., et al., 2012. Quantification of serotonin transporter availability with [11c]Madam — a comparison between the Ecatt Hrrt and Hr systems. *Neuroimage* 60, 800–807.
- Spies, M., et al., 2015. The serotonin transporter in psychiatric disorders: insights from pet imaging. *Lancet Psychiatry* 2, 743–755.
- Tang, Y., et al., 2001. Brain volume changes on longitudinal magnetic resonance imaging in normal older people. *J. Neuroimaging* 11, 393–400.
- Terry, R.D., 2000. Cell death or synaptic loss in Alzheimer disease. *J. Neuropathol. Exp. Neurol.* 59, 1118–1119.
- Tuulari, J.J., et al., 2016. Bariatric surgery induces white and grey matter density recovery in the morbidly obese: a voxel-based morphometric study. *Hum. Brain Mapp.*
- Van Dyck, C.H., et al., 2000. Age-related decline in central serotonin transporter availability with I-123 beta-Cit Spect. *Neurobiol. Aging* 21, 497–501.
- Van Velden, F.H.P., et al., 2015. Comparison of Hrrt and Hr+ scanners for quantitative (R)-[11c]Verapamil, [11c]Raclopride and [11c]Flumazenil brain studies. *Mol. Imaging Biol.* 17, 129–139.
- Volkow, N.D., et al., 2009. Imaging Dopamine's role in drug abuse and addiction. *Neuropharmacology* 56, 3–8.
- Wang, G.J., et al., 2001. Brain dopamine and obesity. *Lancet* 357, 354–357.
- Whone, A.L., et al., 2003. Slower progression of Parkinson's Disease with ropinirole versus levodopa: the real-pet study. *Ann. Neurol.* 54, 93–101.
- Woodward, N.D., et al., 2009. Cerebral morphology and dopamine D2/D3 receptor distribution in humans: a combined [18f]Fallypride and voxel-based morphometry study. *Neuroimage* 46, 31–38.
- Zatorre, R.J., et al., 2012. Plasticity in gray and white: neuroimaging changes in brain structure during learning. *Nat. Neurosci.* 15, 528–536.
- Zubieta, J.K., et al., 1999. Gender and age influences on human brain Mu-opioid receptor binding measured by pet. *Am. J. Psychiatry* 156, 842–848.